

Supplementary Information for

Co-existence of Physisorbed and Solvated HCl at Warm Ice Surfaces

Xiangrui Kong^{,†,‡}, Astrid Waldner^{†,§}, Fabrizio Orlando[†], Luca Artiglia[†], Thomas
Huthwelker[†], Markus Ammann[†], and Thorsten Bartels-Rausch^{*,†}*

AFFILIATIONS

[†]Laboratory of Environmental Chemistry, Paul Scherrer Institute, CH-5232 Villigen PSI, Switzerland

[‡]Department of Chemistry and Molecular Biology, University of Gothenburg, SE-41296 Gothenburg, Sweden

[§]Department of Environmental System Science, ETH Zürich, CH-8092 Zürich, Switzerland

[†]Swiss Light Source, Paul Scherrer Institute, CH-5232, Villigen PSI, Switzerland

AUTHOR INFORMATION

Corresponding Authors

*Xiangrui Kong, xiangrui.kong@chem.gu.se (XK); Thorsten Bartels-Rausch, thorsten.bartels-rausch@psi.ch (TBR).

This file includes:

Materials and Methods
Text S1 to S10
Fig. S1 to S5
Caption for Movie S1
References

Other Supplementary Materials for this manuscript includes the following:

Movie S1

Materials and Methods

The experiments were performed at the SIM and PHOENIX beamlines of the Swiss Light Source (SLS) at Paul Scherrer Institute (PSI), using the near ambient pressure photoelectron (NAPP) spectroscopy end station³. Fig. S1 shows the schematic view of (A) the in-situ cell connected with flow tubes, and (B) the sample holder.

Before the experiments, the cell had been kept in ultra-high vacuum (UHV) condition. Water vapor is dosed via a stainless steel capillary of 800 μm inner diameter from a temperature controlled water reservoir. The water source (Fluka TraceSelect Ultra; Water ACS reagent, for ultra-trace analysis) was degassed by 3 freeze-pump-thaw cycles. The water reservoir was set at 258 K, which gave a pressure about 1 mbar in the cell to keep ice stable at 253 K during the experiments. To trigger the single crystal ice nucleation, the sample holder was cooled down, by cold nitrogen gas that went through liquid nitrogen bath, to obtain the critical supersaturation. Each step of lowering temperature is subtle, to avoid the formation of polycrystalline ice. At the onset of ice nucleation, the pressure in the cell was observed to decline because more gas molecules from the gas phase condense to grow the ice than are desorbed. The ice crystals were kept under this slight oversaturation to grow smoothly until covering the major part of the sample holder. Then, the sample holder was warmed up back to 253 K where the measured pressure matched the initial pressure before ice nucleation occurred. The ice sample is thus kept in equilibrium during experiments. The HCl was dosed from a gas bottle (Messer, 500 ppm HCl in N₂ 5.0) through a calibrated leak valve. The total pressure of HCl/N₂ mixture was

0.15 mbar for the depth profile and NEXAFS measurements. As HCl is sticky gas, which can be significantly depleted by inner walls of the apparatus, in the main text we estimated the local HCl pressure based on the HCl and Cl⁻ surface coverages obtained by XPS data. The local HCl pressure was in the range of 10⁻⁷ mbar during DP measurements and the high dosing case in the NEXAFS measurement, and in the low dosing case the HCl pressure was 10 times lower. Measurements were started after introducing HCl vapor for a few hours, when both Cl 1s and O 1s intensities stabilized (fig. S4).

The depth profile experiment was performed at the PHOENIX beamline. This beamline uses two undulators that provide photons in the range 2200 eV - 8000 eV. The beam size at the sample was about 0.1 mm × 0.1 mm. The XPS survey spectrum (Fig. 1C) was acquired with a photon energy of 2200 eV, and the Chloride 1s peak (Fig. 1D) was measured at PE = 3090 eV as one of the depth profile data points. For the depth profile, the Cl 1s spectrum was measured at the following photon energies: 3090 eV, 3340 eV, 4000 eV, 5000 eV, and 6000 eV. The NEXAFS and additional XPS measurements were carried out at the SIM beamline, which is capable of an energy range of 250 eV - 1500 eV, with a beam size of about 0.1 mm × 0.05 mm at the sample spot. The Cl 2p (Fig. 1E) was measured with a photon energy of 420 eV, and the Cl 2p for NaCl solution (Fig. 1F) was measured at PE = 2200 eV at the PHOENIX beamline as a parallel project. Partial electron yield NEXAFS spectra were acquired at the oxygen K-edge in partial electron yield mode using a kinetic energy window of 450 eV - 470 eV, corresponding to the background of the oxygen Auger line. All spectra were normalized to the incident beam

flux determined from the electron current measured on the last mirror of the beamline before the endstation.

Supplementary Text

Text S1: Estimation of the Cl/O ratio

According to measurements where Cl and O have same kinetic energy (3184 eV, IMFPs were thus identical, 10 nm), the Cl/O ratio is about $5.0 \cdot 10^{-4} : 1$. From equation (1), it is clear that about 97% of the total photoemission intensity comes from the surface region of thickness 3λ , i.e. from the top 30 nm (at the kinetic energy considered). This value is however much larger than the calculated 9 nm effective thickness where all Cl species are distributed. Because the fraction of Cl species compared to H₂O is very small, we can assume that H₂O is homogeneously distributed, which means that the top 9 nm of ice contributes with a factor of $(e^{-9/10 \cos \theta})=65\%$ to the total O 1s signal. Thus, within the top 9 nm, the Cl/O ratio is $5.0 \cdot 10^{-4} : 0.65 = 7.7 \cdot 10^{-4} : 1$.

The distribution of O is proportional to the thickness of the two layers, i.e. the 1st layer has $d/9 = 1/9 = 0.11$ and the 2nd layer has $(9-1)/9 = 0.89$ of total O in 9 nm.

Also, according to the fitted parameters, in the first layer (0 nm to 1 nm) there are

$$[1 / (1 + R)] \cdot 100\% = [1 / (1 + 0.65)] \cdot 100\% \approx 60\%$$

of total Cl, so (corresponding to $7.7 \cdot 10^{-4} \cdot 60\% = 4.6 \cdot 10^{-4}$), and the other 40% is stored in the 2nd layer (corresponding to $7.7 \cdot 10^{-4} \cdot 40\% = 3.1 \cdot 10^{-4}$).

The HCl/H₂O ratio in the first layer is thereby $4.6 \cdot 10^{-4} : 0.11 = 4.2 \cdot 10^{-3} : 1$. Similarly, the ionic Cl⁻ being the only chlorine species in the second layer, the Cl⁻/O ratio in the second layer is $3.1 \cdot 10^{-4} : 0.89 = 3.4 \cdot 10^{-4} : 1$.

Text S2: Parameters for the E-AIM model

The vapor pressure of the second layer is calculated by using the E-AIM model (Model I). The input parameters are:

T = 253 K;

RH = 1 (for ice);

Result: HCl partial pressure is about $1.4 \cdot 10^{-4}$ mbar, and the molar ratio of Cl and H₂O is $0.57 / (0.57 + 8.9) = 6 \cdot 10^{-2} : 1$.

Text S3: Estimation of local HCl pressure above ice

The total pressure of the HCl/N₂ mixture (500 ppm HCl in N₂) is 1.5 mbar, but it is unreasonable to simply estimate the local HCl pressure by the molar ratio and total pressure, because the loss to walls during transportation is a major sink for the sticky gas HCl. It took hours to reach a stabilized Cl to O molar ratio on the ice surface but the total pressure always remains constant. The experiments were carried out in a very low Cl to O

ratio as shown in figure 3. According to the quantitative XPS information of the surface coverage, we estimate the local pressure as follows. The molar ratio of chlorine to H₂O is $\sim 4.2 \cdot 10^{-3} : 1$ for 1st layer and $\sim 3.4 \cdot 10^{-4} : 1$ for 2nd layer (text S9), which corresponds to an apparent HCl surface coverage of $\sim 8\%$ at 253 K. By extrapolating the recently reported apparent Langmuir constant measured between 190 K - 220 K⁴ to 253 K, an HCl partial pressure of 10^{-8} mbar establishes such a surface coverage. However, this back-of-the-envelope calculation is highly uncertain due to the crude extrapolations required. Further, beam induced depletion at the sample spot might contribute to a reduced Cl/O molar ratio compared to other regions of the ice sample.

According to the E-AIM aerosol thermodynamics model^{5,6}, the Cl⁻ to H₂O ratio of a solution on the liquid/solid phase boundary at 253 K is about $6.0 \cdot 10^{-2} : 1$, with an HCl partial pressure of $1.4 \cdot 10^{-4}$ mbar (text S10). Because the molar ratios of Cl to O in the two layers are lower than that of the saturated solution by 1-2 orders of magnitudes, a real local pressure no higher than 10^{-6} mbar seems reasonable.

Thus, the local HCl partial pressure is constrained to $<10^{-6}$ to 10^{-8} mbar, and for the convenience of readers we use 10^{-7} mbar here as the best estimate.

Text S4: Three layer model

The intensity of the photo-emitted electrons for a homogeneous sample is described as,

$$I(x) = I_0 e^{-x/\lambda \cdot \cos\theta} \quad (1)$$

where λ is the inelastic mean free path, x is the depth, θ is the take-off angle at which electrons are detected, I_0 is the photoemission signal intensity in absence of attenuation ($\theta = 30$ degree in our experiments).

Three components are allowed to be in the first layer, which are molecular HCl, ionic Cl^- , and H_2O of ice. Only taking account of chloride containing species and normalizing the sum of them to unity we have,

$$n(\text{HCl}) + n(\text{Cl}_{1st}^-) = 1 \quad (2)$$

where $n(\text{HCl})$ and $n(\text{Cl}_{1st}^-)$ are the fractions of HCl and Cl^- in a unit volume, respectively.

In the second layer, Cl^- is the only Cl containing species. A parameter R is used to represent the relative amount of chlorine species between the two layers,

$$\frac{n(\text{Cl}_{2nd}^-)}{n(\text{HCl}) + n(\text{Cl}_{1st}^-)} = n(\text{Cl}_{2nd}^-) = R \quad (3)$$

No Cl^- containing species diffuse into the third layer (bulk), thus it is pure ice.

The total photoemission signal is given by integrating the contributions over the sample thickness,

$$\int I(x) dx = \int I_0 \cdot e^{-x/\lambda \cdot \cos\theta} dx$$

$$= \lambda \cdot \cos\theta \cdot I_0 \cdot e^{-x/\lambda \cdot \cos\theta} \quad (4)$$

Applying eq (4) to integrate the signals from the first layer (from depth d to 0), we have

$$\begin{aligned} I_{1st} &= \lambda \cdot \cos\theta \cdot I_0 \cdot e^{-0/\lambda \cdot \cos\theta} - \lambda \cdot \cos\theta \cdot I_0 \cdot e^{-d/\lambda \cdot \cos\theta} \\ &= \lambda \cdot \cos\theta \cdot I_0 \cdot (1 - e^{-d/\lambda \cdot \cos\theta}) \end{aligned} \quad (5)$$

Integration of the second layer is from depth x from D to d ,

$$\begin{aligned} I_{2nd} &= \lambda \cdot \cos\theta \cdot I_0 \cdot e^{-d/\lambda \cdot \cos\theta} - \lambda \cdot \cos\theta \cdot I_0 \cdot e^{-D/\lambda \cdot \cos\theta} \\ &= \lambda \cdot \cos\theta \cdot I_0 (e^{-d/\lambda \cdot \cos\theta} - e^{-D/\lambda \cdot \cos\theta}) \end{aligned} \quad (6)$$

We now look at HCl and Cl⁻, respectively. As HCl only exists in the first layer, the HCl signal is

$$\begin{aligned} I_{HCl} &= n(HCl) \cdot I_{1st} \\ &= n(HCl) \cdot \lambda \cdot \cos\theta \cdot I_0 \cdot (1 - e^{-d/\lambda \cdot \cos\theta}) \end{aligned} \quad (7)$$

The ionic Cl⁻ signals are from both of the first and second layer,

$$\begin{aligned} I_{Cl^-} &= n(Cl_{1st}^-) \cdot I_{1st} + n(Cl_{2nd}^-) \cdot I_{2nd} \\ &= n(Cl_{1st}^-) \cdot \lambda \cdot \cos\theta \cdot I_0 \cdot (1 - e^{-d/\lambda \cdot \cos\theta}) + R \cdot \lambda \cdot \cos\theta \cdot I_0 \cdot (e^{-d/\lambda \cdot \cos\theta} - e^{-D/\lambda \cdot \cos\theta}) \\ &= \lambda \cdot \cos\theta \cdot I_0 \cdot [n(Cl_{1st}^-) \cdot (1 - e^{-d/\lambda \cdot \cos\theta}) + R \cdot (e^{-d/\lambda \cdot \cos\theta} - e^{-D/\lambda \cdot \cos\theta})] \end{aligned} \quad (8)$$

Combining eqs (7) and (8), the ratio of HCl and Cl⁻ at a same KE will be

$$\begin{aligned}
\frac{I_{HCl}}{I_{Cl^-}} &= \frac{n(HCl) \cdot \lambda \cdot \cos \theta \cdot I_0 \cdot (1 - e^{-d/\lambda \cdot \cos \theta})}{\lambda \cdot \cos \theta \cdot I_0 \cdot \left[n(Cl_{1st}^-) \cdot (1 - e^{-d/\lambda \cdot \cos \theta}) + R \cdot (e^{-d/\lambda \cdot \cos \theta} - e^{-D/\lambda \cdot \cos \theta}) \right]} \\
&= \frac{n(HCl) \cdot (1 - e^{-d/\lambda \cdot \cos \theta})}{n(Cl_{1st}^-) \cdot (1 - e^{-d/\lambda \cdot \cos \theta}) + R \cdot (e^{-d/\lambda \cdot \cos \theta} - e^{-D/\lambda \cdot \cos \theta})} \\
&= \frac{n(HCl) \cdot (1 - e^{-d/\lambda \cdot \cos \theta})}{n(Cl_{1st}^-) + [R - n(Cl_{1st}^-)] \cdot e^{-d/\lambda \cdot \cos \theta} - R \cdot e^{-D/\lambda \cdot \cos \theta}} \tag{9}
\end{aligned}$$

According to eq (7), relative HCl intensities measured at different photon energies can be written as

$$\begin{aligned}
\frac{I_{HCl}(KE)}{I_{HCl_ref}} &= \frac{n(HCl) \cdot \lambda(KE) \cdot \cos \theta \cdot I_0 \cdot (1 - e^{-d/\lambda(KE) \cdot \cos \theta})}{n(HCl) \cdot \lambda_{ref} \cdot \cos \theta \cdot I_0 \cdot (1 - e^{-d/(\lambda_{ref} \cdot \cos \theta)})} \\
&= \frac{\lambda(KE) \cdot (1 - e^{-d/\lambda(KE) \cdot \cos \theta})}{\lambda_{ref} \cdot (1 - e^{-d/\lambda_{ref} \cdot \cos \theta})} \tag{10}
\end{aligned}$$

where KE is the kinetic energy yielded from different photon energy, $\lambda(KE)$ is a function of KE , I_{HCl_ref} refers to the HCl intensity measured by a reference photon energy, and λ_{ref} is the IMFP corresponding to the reference kinetic energy. In order to mimic the relative density as shown in Fig. 2(A), the intensities here were normalized to their IMFP, respectively. Thus, the relative density of HCl becomes

$$\frac{Den_{HCl}(KE)}{Den_{HCl_ref}} = \frac{1 - e^{-d/\lambda(KE)\cos\theta}}{1 - e^{-d/(\lambda_{ref}\cos\theta)}} \quad (11)$$

Similarly, from eq (8) relative Cl⁻ intensities measured at different photon energies can be written as

$$\begin{aligned} \frac{I_{Cl^-}(KE)}{I_{Cl^-_ref}} &= \frac{\lambda(KE) \cdot \cos\theta \cdot I_0 \cdot [n(Cl_{1st}^-) \cdot (1 - e^{-d/\lambda(KE)\cos\theta}) + R \cdot (e^{-d/\lambda(KE)\cos\theta} - e^{-D/\lambda(KE)\cos\theta})]}{\lambda_{ref} \cdot \cos\theta \cdot I_0 \cdot [n(Cl_{1st}^-) \cdot (1 - e^{-d/\lambda_{ref}\cos\theta}) + R \cdot (e^{-d/\lambda_{ref}\cos\theta} - e^{-D/\lambda_{ref}\cos\theta})]} \\ &= \frac{n(Cl_{1st}^-) \cdot \lambda(KE) \cdot (1 - e^{-d/\lambda(KE)\cos\theta}) + R \cdot \lambda(KE) \cdot (e^{-d/\lambda(KE)\cos\theta} - e^{-D/\lambda(KE)\cos\theta})}{n(Cl_{1st}^-) \cdot \lambda_{ref} \cdot (1 - e^{-d/\lambda_{ref}\cos\theta}) + R \cdot \lambda_{ref} \cdot (e^{-d/\lambda_{ref}\cos\theta} - e^{-D/\lambda_{ref}\cos\theta})} \end{aligned} \quad (12)$$

And, the relative density of Cl⁻ is

$$\frac{Den_{Cl^-}(KE)}{Den_{Cl^-_ref}} = \frac{n(Cl_{1st}^-) \cdot (1 - e^{-d/\lambda(KE)\cos\theta}) + R \cdot (e^{-d/\lambda(KE)\cos\theta} - e^{-D/\lambda(KE)\cos\theta})}{n(Cl_{1st}^-) \cdot (1 - e^{-d/\lambda_{ref}\cos\theta}) + R \cdot (e^{-d/\lambda_{ref}\cos\theta} - e^{-D/\lambda_{ref}\cos\theta})} \quad (13)$$

The fitting was done in a non-linear least square fashion to minimize global residual of three depth profiles by using eqs (9), (11) and (13). Note that the depth profiles of HCl and Cl⁻ are normalized to the first point, thus the reference IMFP (λ_{ref}) in eqs (10) and (11) corresponds to that of the first data point (Photon Energy = 3090 eV, Kinetic Energy = 274 eV). The HCl/Cl⁻ ratio does not need any correction procedure to account for the experimental setup, because it is calculated directly from the ratio between the XPS areas of molecular and ionic peaks in the Cl 1s spectra. Regarding this last point, we have to

specify that we applied an internal normalization to the reference as we always measured a reference and the DP points at the same sample spot.

Text S5: Probing depth

The probing depth (D_p) is calculated as the product of inelastic free mean path (IMFP)^{1,7,8} and the cosine of take-off angle (θ), i.e. $D_p = \text{IMFP} \cdot \cos(\theta)$, where $\theta = 30^\circ$.

Text S6: Ice stability and measurements strategy

The signal intensity in high-pressure XPS is a critical function of the distance between the sample and the inlet of the differential pumping stage of the analyzer (working distance). In order to minimize the variation in working distance between the individual sampling spots for each depth profile data point, we always took reference measurements at fixed photon energy before and after each DP measurement. The reference is also used to monitor the stability of the working distance and thus to ensure that the ice sample was neither growing nor evaporating during each individual measurement. Fig. S4 shows the good stability of Cl 1s and O 1s before (solid line) and after (dotted line) each DP measurement. These reference measurements further demonstrate that the total amount of chlorine and the ratio of HCl to Cl⁻ did not change during the measurement time. To acquire a DP data point took about 5 minutes. The reference was measured at 3340 eV.

The DP measurements are based on 2 independent experiments with similar surface coverage but different dosing history. The first DP is with an initial total HCl/N₂ pressure

measured as $1.5 \cdot 10^{-1}$ mbar, where the HCl-N₂ mixture were dosed into a clean chamber that was free of HCl. The second DP is with an HCl/N₂ measured partial pressure of $0.5 \cdot 10^{-1}$ mbar, where the chamber had been exposed to higher HCl pressure. Due to the memory effects in the system, the ice in the two DPs seems to have similar HCl surface coverages, as the HCl/Cl⁻ ratio seems to be a function of local HCl partial pressure/surface coverage. The actual orders of the two measurements were: 1) DP4-DP2-DP3-DP5-DP1; 2) DP3-DP4-DP5-DP1-DP2 to avoid artefacts that may arise from time-dependent trends.

The NEXAFS measurements were optimized for shortest possible measurement time of not more than 30 min to minimize potential changes during beam exposure. Spectra were recorded in the photon energy range of 525 eV to 560 eV. In Figure 4, the measurement of spectrum (B) started from 525 eV, and the spectra (C) and (D) were recorded from the 560 eV.

Text S7: XPS data processing

Before plotting the depth profile data, normalization were performed so that the photoelectron intensities obtained at different kinetic energy can be compared. The normalization process includes (1) photoionization cross section⁹, to account for the ionization efficiency at different photon energy; (2) inelastic free mean path (IMFP) in ice^{1,7,8}, to normalize the different probing depths at different kinetic energies; (3) X-ray photon flux, to account for beam intensity fluctuations; (4) transmission of the electron

analyser, to account for detection efficiency at different electron kinetic energies. The spectra were fitted with Gaussians functions and a linear background. The binding energy scale was referenced to the O 1s core level peak at 535 eV. Such core level XPS spectra were recorded for this purpose for each Cl 1s spectrum at the same photon energy.

Text S8: Sensitivity analysis of depth profiles on IMFPs

The IMFP values used in the DP normalization are from previous studies of ice and water^{1,7,8}. Due to the considerable uncertainty of IMFP^{2,7,10,11}, we performed sensitivity analysis of IMFP impacting on the DP data. Assuming the IMFPs are linearly correlated to kinetic energy, the slope of the IMFP was increased by 20%, 40%, 60%, 80% (fig. S5), which were between the values from previous studies^{1,2}.

Fig. S5 generally shows a strong decrease of the measured cumulative Cl⁻ and HCl normalized concentration with KE as the slope of IMFP increases. The ratio of HCl/Cl⁻ is not shown because it is not affected by IMFP. When approaching the IMPF in water, the HCl depth profile becomes significantly steeper, while the one of Cl⁻ mainly levels off in the initial part.

The fitting results from the sensitivity test are shown in fig. S6. In each panel, three cases of d were compared: 1) $d = 0.5$ nm; 2) $d = 1$ nm; 3) freely fitted d , where d always locates between 1.5 nm and 2 nm. The free d case gives the minimum overall residue of three DP, but due to the worse fitting to the HCl/Cl⁻ ratio (the most certain data set, no

normalization was needed) it is regarded as the worst fitting compared to the other two cases.

No significant differences of the fitting outcome were seen. The border of the second layer is always around 10 nm, and the first layer depth was 0.5 nm - 1.5 nm.

An interesting point is that in higher IMFP cases, the first layer was assigned with some Cl⁻ fraction. Thus, a minor amount of Cl⁻ might be present in the first layer, regarding the uncertainty of IMFP.

Text S9: Estimation of binding energy between molecular HCl and ice

Impingement rate (F) is written as

$$F = \frac{P}{\sqrt{2\pi \cdot m \cdot k_b \cdot T}} \quad (14)$$

where P is partial pressure, m is atomic mass unit, k_b is Boltzmann constant, T is temperature.

The residence time of HCl on ice is

$$\tau = \frac{S \cdot C}{F} = \frac{S \cdot C \cdot \sqrt{2\pi \cdot m \cdot k_b \cdot T}}{P} \quad (15)$$

where S is saturated surface density, C is HCl surface coverage.

$$S \approx 10^{15} \text{ molecules} \cdot \text{cm}^{-2}$$

$$C \approx 4 \cdot 10^{-3}$$

As discussed in the main text, P may be in the range of $1 \cdot 10 \cdot 10^{-7}$ mbar, where the residence time is corresponding to 8.2 ms to 0.82 ms.

From the Arrhenius equation,

$$k = A \cdot e^{-E/R.T} \quad (16)$$

where k is desorption rate constant ($1/\tau$), A is pre-exponential factor, E is activation energy of desorption, R is ideal gas constant. By assuming a pre-exponential factor A as 10^{13} for an ordinary desorption process¹², the binding energy of non-dissociated HCl on ice can be determined in the range from 48.0 kJ/mol to 52.9 kJ/mol. By allowing A changes by $\pm 50\%$ as uncertainty range, the binding energy is ranged from 51.4 kJ/mol to 56.2 kJ/mol (+50%) and 46.6 kJ/mol to 51.4 kJ/mol. Such binding energy indicates that HCl forms slightly more than 2 hydrogen bonds with ice surface.

Text S10: Carbon contamination in NEXAFS

The oxygen K-edge NEXAFS was taken in the SIM beamline because of the applicable X-ray photon energy range. Carbon signal was visible during the measurement, but no

consequences or changes to the system were observed compared to other carbon-free measurements in this beamline or the other beamline, i.e. PHOENIX.

A dominating effect of the carbon contamination on the pre-melting can be ruled out based on the following evidence: (1) In Figure 3 of ¹³, NEXAFS spectra with a similar level of contamination peak intensity show only a minor change in the NEXAFS spectra compared to the spectra in presence of HCl reported here. (2) We studied the pre-melting of ice in presence of formic acid (unpublished results). Strong changes to the NEXAFS spectrum are, even for this strong carboxylic acid, only seen when intensity at 532.5 eV (reflecting the presence of formic acid and potential contamination) is much higher than seen in the work reported here. On the other hand, surface disorder caused by HCl is in full agreement to pioneering work by McNeill et al. (2006).

Bluhm *et al.*¹³ discussed the carbon contamination issue and its effect on the oxygen K-edge NEXAFS of ice and suggested that a trace-level amount of carbon comparable to that in our experiment does not have influence on the ice surface disorder. Further, to our knowledge, in order to cause phase change of ice at 253 K, the strongest carbocyclic acid, formic acid, needs a partial pressure in the range of 10^{-2} mbar¹⁴, which is higher than needed for HCl ($1.4 \cdot 10^{-4}$ mbar) by more than 2 orders of magnitudes. We studied the pre-melting of ice in presence of formic acid (unpublished results). Strong changes to the NEXAFS spectrum are, even for this strong carboxylic acid, only seen when intensity at 532.5 eV (reflecting the presence of formic acid and potential contamination) is much higher than seen in the work reported here. On the other hand, surface disorder caused by

HCl is in full agreement to pioneering work by McNeill et al. (2006). Thus, the effects of carbon contamination on surface disorder can be excluded.

Fig. S1

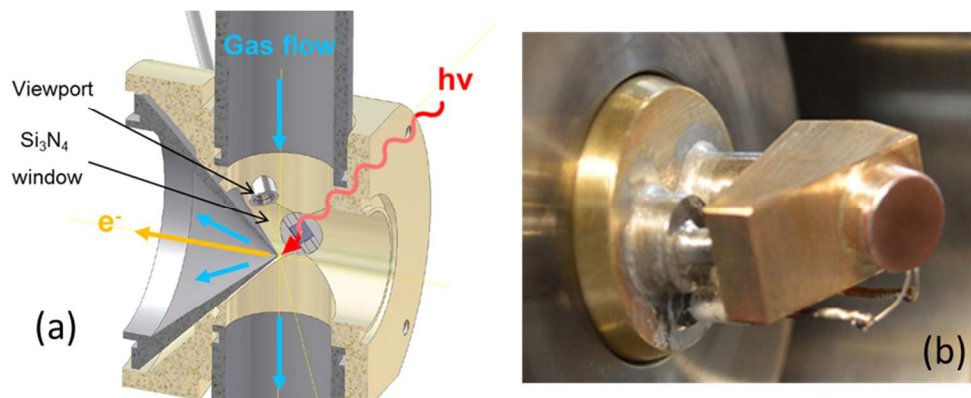


Fig. S1 Schematic view of (a) the in-situ cell, and (b) the sample holder. In (a), the X-ray is directed through the Si₃N₄ window and pointed on the sample holder that is shown in (b). The emitted photoelectrons and Auger electrons went through the cone which interfaces the vacuum and the high pressure sides. The gas flow is indicated. A viewport is located in front of the sample holder, from where the pictures shown in Figure 1 and the movie were taken.

Fig. S2

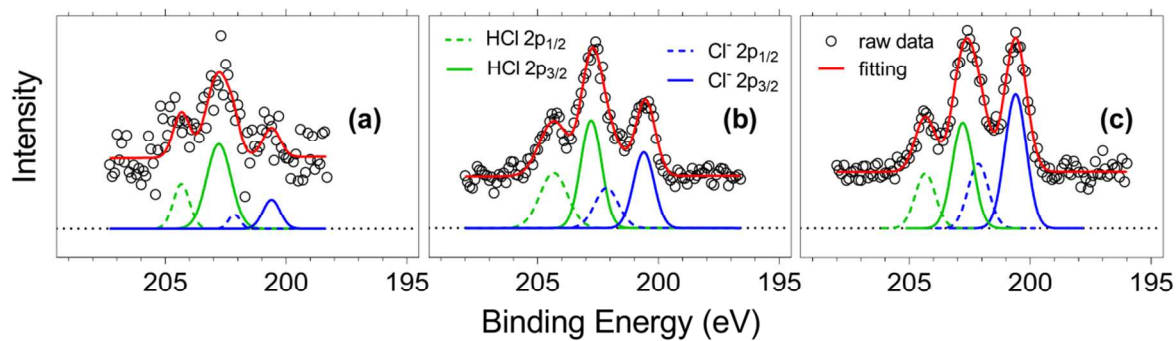


Fig. S2 Chloride 2p core level spectra along with increasing HCl partial pressure at the SIM beamline with 420 eV photon energy. The temperature of the ice was 253 K. The local HCl partial pressures were in the range of 10^{-7} mbar. The partial pressure in (a) is as 1/2 as that in (b) and as 1/8 as that in (c). The HCl/Cl⁻ molar ratios were: (a) 4 : 1; (b) 1.7 : 1; (c) 0.8 : 1.

Fig. S3

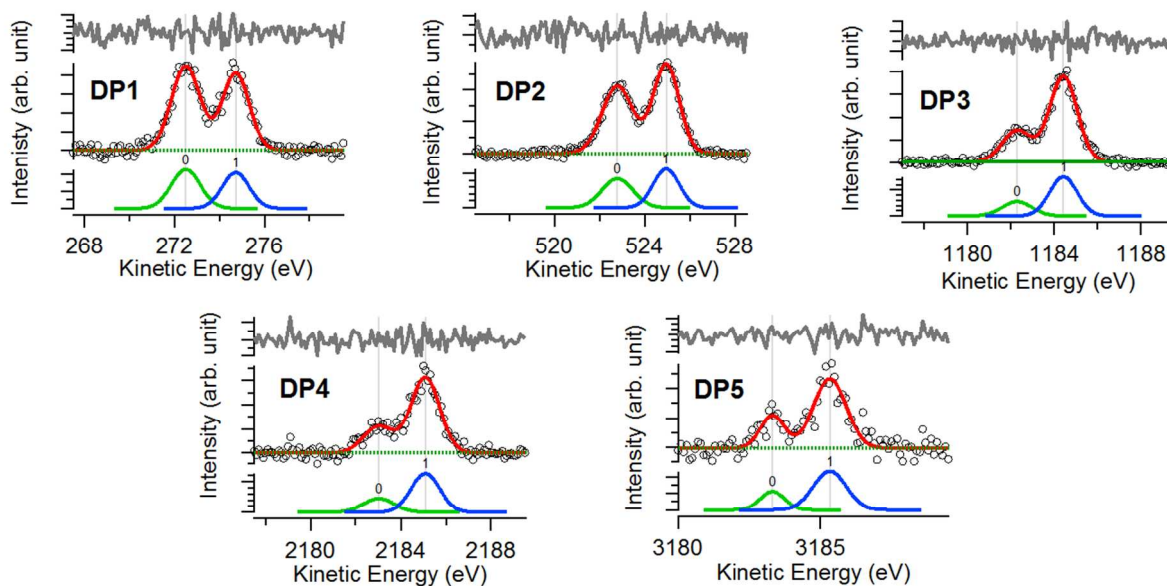


Fig. S3 Illustration of the fittings of Cl 1s used in the depth profile. Note that the normalized process described in supporting information was performed after this fitting process. The circles are raw data; the red curves are the overall fitting; the grey curves are the residue between fitting and raw data; the blue distributions are corresponding to ionic Cl⁻ and the green ones are for molecular HCl.

Fig. S4

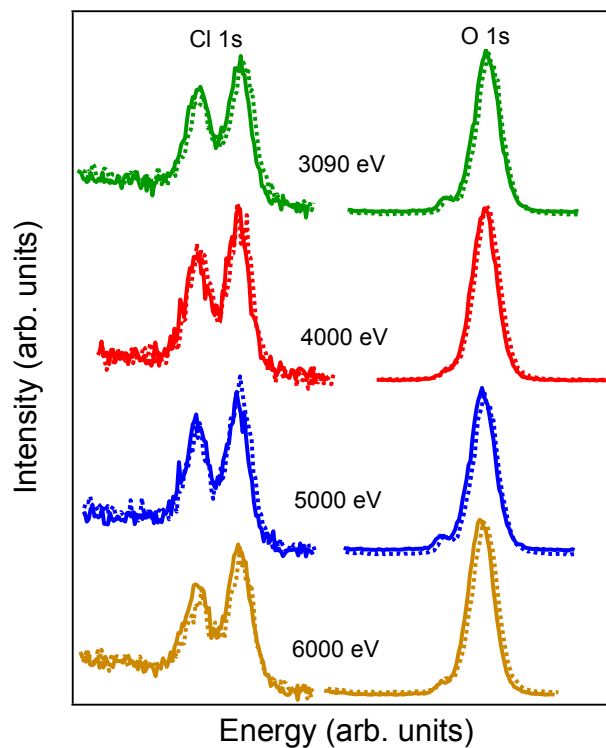


Fig. S4 Reference Cl 1s and O 1s measured at 3340 eV photon energy before (solid line) and after (dotted) depth profile measurements at marked photon energy. Both Cl 1s and O 1s XPS intensities were stable during the measurements.

Fig. S5

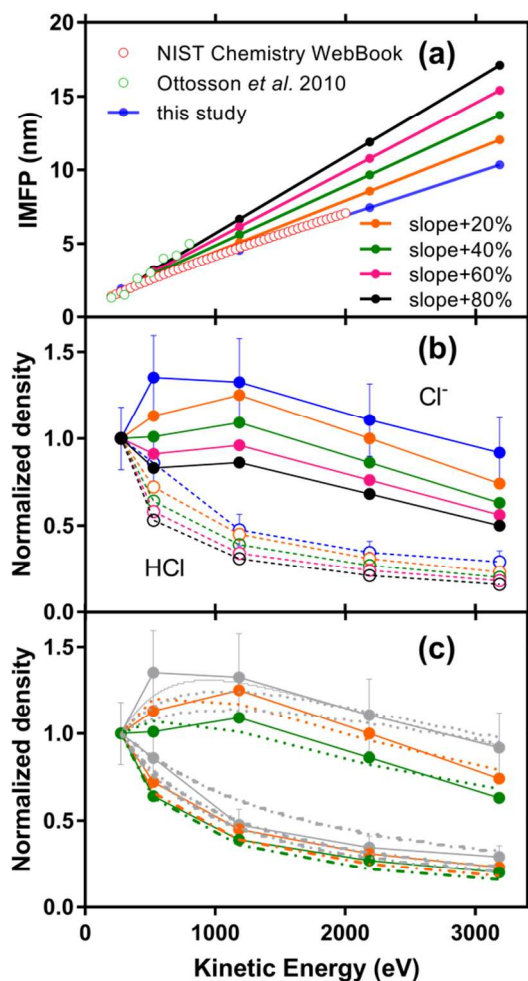


Fig. S5 Sensitivity analysis of the depth profiles for different IMFPs. Panel (a) shows the currently used IMFP in blue, same as that used by Krepelova *et al.*¹ in red empty circles; green empty circles show that from Ottosson *et al.* 2010²; adjusted slopes were indicated in respective colors. Panel (b) shows the depth profiles of HCl and Cl⁻ with different IMFP, indicated by the same colors. Panel (c) shows the fittings results from the layer model, where the grey curves are those shown in the main text (Figure 2) for comparison, and the orange and green ones correspond to +20% and +40% slope cases.

Fig. S6

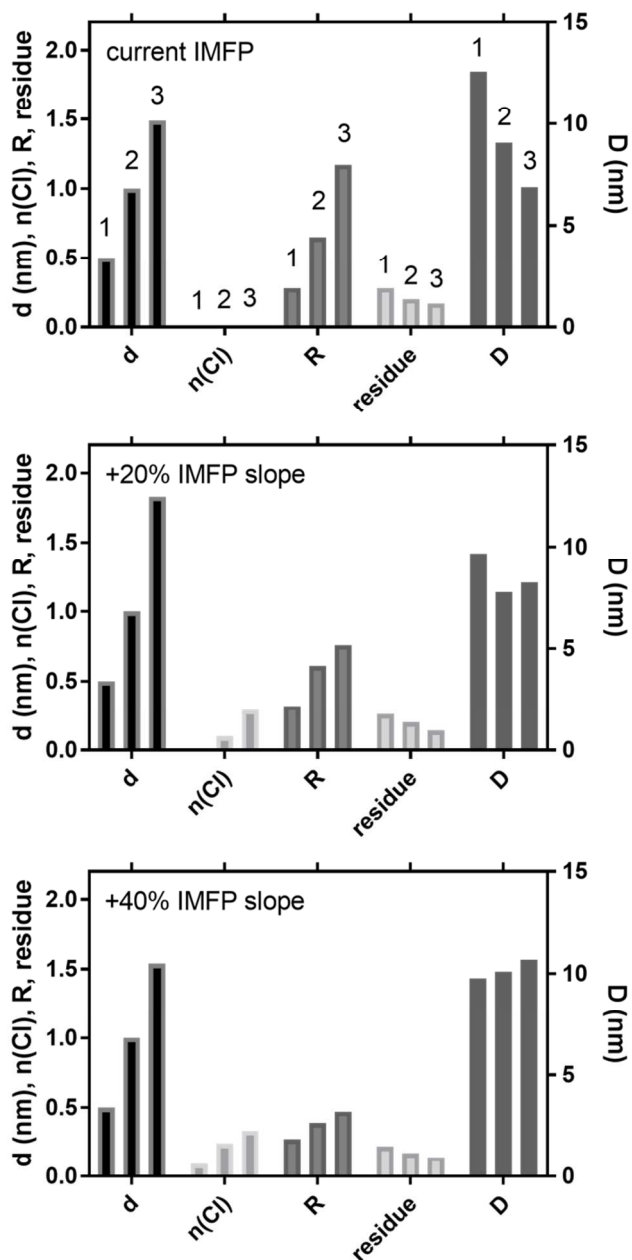


Fig. S6 Fitted parameters from different d values and IMFPs. d is the thickness of the first layer; $n(\text{Cl})$ is the fraction of $\text{Cl}^-/(\text{HCl}+\text{Cl}^-)$ in the first layer; R is the molecular ratio of Cl between the second layer and the first layer; residue is the difference between fitting and actual values; D is the depth where the border of the second layer locates. In each panel, three cases of d were compared, which are represented by number 1 (d is set as 0.5 nm), 2 (d is set as 1.0 nm), 3 (d is freely fitted).

Caption for Movie S1

The growth of single crystal ice on the sample holder in NAPP

References

- (1) Krepelova, A.; Bartels-Rausch, T.; Brown, M. A.; Bluhm, H.; Ammann, M. Adsorption of Acetic Acid on Ice Studied by Ambient-Pressure XPS and Partial-Electron-Yield NEXAFS Spectroscopy at 230-240 K. *J. Phys. Chem. A* **2013**, *117*, 401-409.
- (2) Ottosson, N.; Faubel, M.; Bradforth, S. E.; Jungwirth, P.; Winter, B. Photoelectron Spectroscopy of Liquid Water and Aqueous Solution: Electron Effective Attenuation Lengths and Emission-angle Anisotropy. *J. Electron. Spectrosc.* **2010**, *177*, 60-70.
- (3) Orlando, F.; Waldner, A.; Bartels-Rausch, T.; Birrer, M.; Kato, S.; Lee, M. T.; Proff, C.; Huthwelker, T.; Kleibert, A.; van Bokhoven, J.; *et al.* The Environmental Photochemistry of Oxide Surfaces and the Nature of Frozen Salt Solutions: A New in Situ XPS Approach. *Top. Catal.* **2016**, *59*, 591-604.
- (4) Zimmermann, S.; Kippenberger, M.; Schuster, G.; Crowley, J. N. Adsorption Isotherms for Hydrogen Chloride (HCl) on Ice Surfaces between 190 and 220 K. *Phys. Chem. Chem. Phys.* **2016**, *18*, 13799-13810.
- (5) Massucci, M.; Clegg, S. L.; Brimblecombe, P. Equilibrium Partial Pressures, Thermodynamic Properties of Aqueous and Solid Phases, and Cl₂ Production from Aqueous HCl and HNO₃ and their Mixtures. *J. Phys. Chem. A* **1999**, *103*, 4209-4226.
- (6) Carslaw, K. S.; Clegg, S. L.; Brimblecombe, P. A Thermodynamic Model of the System HCl-HNO₃-H₂SO₄-H₂O, Including Solubilities of HBr, from <200 to 328 K. *J. Phys. Chem.* **1995**, *99*, 11557-11574.
- (7) Nikjoo, H.; Uehara, S.; Emfietzoglou, D.; Brahme, A. Heavy Charged Particles in Radiation Biology and Biophysics. *New J. Phys.* **2008**, *10*, 075006.
- (8) Tanuma, S.; Powell, C. J.; Penn, D. R. Calculations of Electron Inelastic Mean Free Paths. VIII. Data for 15 Elemental Solids over the 50-2000 eV range. *Surf. Interface Anal.* **2005**, *37*, 1-14.
- (9) Trzhaskovskaya, M. B.; Nefedov, V. I.; Yarzhemsky, V. G. Photoelectron Angular Distribution Parameters for Elements Z=1 to Z=54 in the Photoelectron Energy Range 100–5000 eV. *Atomic Data and Nuclear Data Tables* **2001**, *77*, 97-159.
- (10) Suzuki, Y. I.; Nishizawa, K.; Kurahashi, N.; Suzuki, T. Effective Attenuation Length of an Electron in Liquid Water between 10 and 600 eV. *Phys. Rev. E* **2014**, *90*, 010302.
- (11) Thürmer, S.; Seidel, R.; Faubel, M.; Eberhardt, W.; Hemminger, J. C.; Bradforth, S. E.; Winter, B. Photoelectron Angular Distributions from Liquid Water: Effects of Electron Scattering. *Phys. Rev. Lett.* **2013**, *111*, 173005.
- (12) Kong, X. R.; Papagiannakopoulos, P.; Thomson, E. S.; Markovic, N.; Pettersson, J. B. C. Water Accommodation and Desorption Kinetics on Ice. *J. Phys. Chem. A* **2014**, *118*, 3973-3979.
- (13) Bluhm, H.; Ogletree, D. F.; Fadley, C. S.; Hussain, Z.; Salmeron, N. The Premelting of Ice Studied with Photoelectron Spectroscopy. *J. Phys. Condens. Mat.* **2002**, *14*, L227-L233.

- (14) Lide, D. R.: *CRC handbook of chemistry and physics: a ready-reference book of chemical and physical data*; 85th ed.; CRC Press: Florida, 2004.